HHS Public Access

Author manuscript

Biochemistry. Author manuscript; available in PMC 2018 June 13.

Published in final edited form as:

Biochemistry. 2017 August 15; 56(32): 4201–4209. doi:10.1021/acs.biochem.7b00407.

Structural Insights into Selective Ligand–Receptor Interactions Leading to Receptor Inactivation Utilizing Selective Melanocortin 3 Receptor Antagonists

Minying Cai[*,†,‖], **Udaya Kiran Marelli**[§,‖], **Blake Mertz**[‡,‖], **Johannes G. Beck**[§], **Florian Opperer**[§], **Florian Rechenmacher**[§], **Horst Kessler**[§], and **Victor J. Hruby**[†]

[†]Department of Chemistry and Biochemistry, University of Arizona, Tucson, Arizona 85721, United States

[‡]C. Eugene Bennett Department of Chemistry, West Virginia University, Morgantown, West Virginia 26506, United States

[§]Institute for Advanced Study (IAS) and Center for Integrated Protein Science (CIPSM), Department Chemie, Technische Universität München, 85747 Garching, Germany

Abstract

Systematic N-methylated derivatives of the melanocortin receptor ligand, SHU9119, lead to multiple binding and functional selectivity toward melanocortin receptors. However, the relationship between N-methylation-induced conformational changes in the peptide backbone and side chains and melanocortin receptor selectivity is still unknown. We conducted comprehensive conformational studies in solution of two selective antagonists of the third isoform of the melanocortin receptor (hMC3R), namely, Ac-Nle-c[Asp-*N*Me-His^6-D-Nal(2')^7-*N*Me-Arg^8-Trp^9-Lys]-NH_2 (**15**) and Ac-Nle-c[Asp-His^6-D-Nal(2')^7-*N*Me-Arg^8-*N*Me-Trp^9-*N*Me-Lys]-NH_2 (**17**). It is known that the pharmacophore (His^6-DNal^7-Arg^8-Trp^9) of the SHU-9119 peptides occupies a β II-turn-like region with the turn centered about DNal^7-Arg^8. The analogues with hMC3R selectivity showed distinct differences in the spatial arrangement of the Trp^9 side chains. In addition to our NMR studies, we also carried out molecular-level interaction studies of these two peptides at the homology model of hMC3R. Earlier chimeric human melanocortin 3 receptor studies revealed insights regarding the binding and functional sites of hMC3R selectivity. Upon docking of peptides **15** and **17** to the binding pocket of hMC3R, it was revealed that Arg^8 and Trp^9 side chains are involved in a majority of the interactions with the receptor. While Arg^8 forms polar contacts with D154 and D158 of hMC3R, Trp^9 utilizes π–π stacking interactions with F295 and

[*]Corresponding Author: 1306 E. University Blvd, Tucson, AZ 85721. Phone: 520-621-8617. Fax: 520-621-8617. mcai@u.arizona.edu.

[‖]**Author Contributions**

M.C., U.K.M., and B.M. contributed equally to this work.

ORCID

Minying Cai: 0000-0001-9504-2091

Blake Mertz: 0000-0002-7677-0496

Notes

The authors declare no competing financial interest.

Supporting Information

The Supporting Information is available free of charge on the ACS Publications website at DOI: 10.1021/acs.bio-chem.7b00407.

HPLC data, bioassay data, and NMR analysis data (PDF)

F298, located on the transmembrane domain of hMC3R. It is hypothesized that as the frequency of Trp^9-hMC3R interactions decrease, antagonistic activity increases. The absence of any interactions of the *N*-methyl groups with hMC3R suggests that their primary function is to modulate backbone conformations of the ligands.

Graphical Abstract

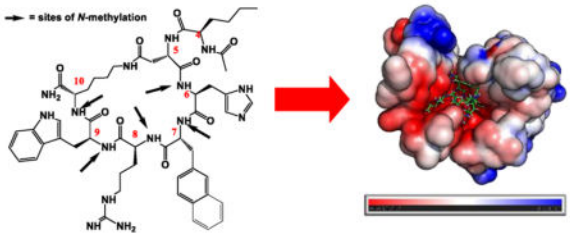

The melanocortin system remains a challenging target for rational peptide and peptidomimetic design as the 3D-topographical requirements for specific melanocortin receptor subtype recognition and activation have not been fully elucidated.[1,2] Nevertheless, the numerous physiological functions of the five known subtypes of human melanocortin receptors (hMC1–5R), including skin pigmentation,[3–6] control of the immune system,[7,8] erectile function,[9] blood pressure and heart rate,[10,11] control of feeding behavior and energy homeostasis,[3,12–16] modulation of aggressive/defensive behavior,[17,18] mediation of pain,[19–23] and control of neurodegenerative diseases, provide a strong stimulus for the development of potent and selective melanocortin agonists and antagonists. On the other hand, development of selective ligands to melanocortin receptors bears intrinsic challenges due to conserved amino acid sequences and their structural similarity contained in the 7 transmembrane fold of G protein-coupled receptors (GPCRs).[24]

Unlike other GPCRs, the human melanocortin system utilizes both endogenous natural agonists (MSHs, including α-MSH, β-MSH, and γ-MSH)[25] and antagonist (AGRP) molecules for functional regulation.[26,27] Interestingly, the primary core sequences of MSHs (His-Phe-Arg-Trp-) and AGRP (-Phe-Phe-Asn-Phe-) are different.[28] This aspect of different activity suggests that the structural differences of melanocortin ligands facilitate selectivity to receptor subtype in addition to functioning as an agonist (MSH) or antagonist (AGRP). Studies on chimeric hMCRs revealed that the binding of NDP-α-MSH to hMC4R is controlled by conserved amino acids with the protein.[29–32] However, the binding interactions of hMC4R with the small molecule, THIQ, are different: both conserved amino acids and nonconserved amino acids of hMC4R are involved in the binding complex.[32] Furthermore, follow up studies demonstrated that peptide agonists and small molecular agonists activate different downstream signaling pathways.[33–36] These discoveries imply that peptide agonists which mimic the natural endogenous peptide ligand will subsequently mimic more closely the natural signaling pathways, thus avoiding potential side effects associated with pharmaceutical applications. In this regard, the study of peptide interactions with hMCRs is of critical importance to identify selective ligand–receptor binding and activation.

Previous studies utilized multiple N-methylations of α-MSH Ac-Nle-c[Asp^5, D-Nal(2')^7, Lys^{10}]-α-MSH-NH_2 (SHU9119) to identify ligands of all subtypes of selective melanotropins.[37] To further develop our fundamental understanding of receptor–ligand interactions that contribute to receptor selectivity and activation, we performed comprehensive conformational studies of two peptides selective for hMC3R. These two peptides are N-methylated derivatives of SHU9119, (Ac-Nle-c[Asp-*N*Me-His^6-D-Nal(2')^7-*N*Me-Arg^8-Trp^9-Lys]-NH_2 (**15**) and Ac-Nle-c[Asp-His^6-D-Nal(2')^7-*N*Me-Arg^8-*N*Me-Trp^9-*N*Me-Lys]-NH_2 (**17**)). (Peptide numbering is based on our previous work.[37]) In addition, earlier studies on chimeric receptors of hMC3R identified six amino acids, important to NDP-α-MSH-hMC3R binding and activation (E131, D154, D158, L165, F295/F296, and H298) (Figure 1);[38] these residues will be used to guide our study of selective ligand–receptor interactions by molecular docking. Although the two peptide ligands have slightly different potency for hMC3R, the interaction sites are similar. Our systematic study of selective ligand–receptor interactions reveals the critical binding and activation sites of the hMC3R. This study will enhance rational drug design and discovery in the future for hMC3R and melanocortin receptors in general.

EXPERIMENTAL METHODS

Peptide Synthesis and Characterization

The synthesis, structural characterization, and pharmacological activity profiles have been previous published.[37]

NMR Conformational Studies

NMR Spectroscopic Studies—For NMR spectroscopic studies, approximately 1.5 to 2 mg of the compound was dissolved in 125 μL of DMSO-d_6. The required NMR spectra were recorded at 300 K on a Bruker 500 MHz spectrometer equipped with a TXI cryoprobe. ^{1}-1D, TOCSY, ROESY, HSQC, and HMBC NMR experiments were acquired for each sample. ^{1}H-Selective homo-nuclear decoupling experiments were carried out to measure ^3J_H couplings. Furthermore, to estimate the solvent shielding or hydrogen bonding strengths of NH protons, the temperature dependency of NH chemical shifts was studied by acquiring ^{1}H-1D spectra between 295 and 315 K in steps of 5 K increments. Mixing times of 80 and 100 ms were used for TOCSY and ROESY experiments, respectively. HSQC spectra were recorded with a direct proton carbon coupling constant of 140 Hz, and HMBC spectra with a long-range ^{1}H–^{13}C coupling constant of 7 Hz. For HSQC spectra, a ^{13}C composite pulse decoupling was utilized. 8k (except HSQC: 1k) data points were recorded in the direct dimension and 384 and 512 (heteronuclear spectra) in the indirect dimension. For all spectra, a 1.5 s relaxation delay was used after every transient. Exponential/square sine window functions were used for spectra apodization.

Proton–Proton Internuclear Distances for Structure Calculation—ROE cross-peaks in corresponding ROESY spectra recorded in various solvents were integrated by using the box method in SPARKY software. These integrated volumes of ROE cross-peaks were converted to proton–proton internuclear distances by a linear approximation method.

Thus, calculated distances were then relaxed by ±10 to generate upper and lower distance bounds to account for experimental and simulation uncertainties.

Distance Geometry (DG) Calculations—Metric matrix DG calculations were carried out with a home-written distance geometry program utilizing random metrization. The above calculated experimental distance restraints which are more restrictive than the geometric distance bounds (holonomic restraints) were used to create the final distance matrix. 50 structures were calculated for each system. The structures were then verified and checked for violations if any with respect to the given experimental distance restraint inputs. The structures that best satisfied the distance inputs were then taken forward for MD simulations.

Molecular Dynamics Studies—All MD simulations were carried out with GROMACS version 4.0.5.[51] The above DG structures served as starting conformations for the MD runs. The charmm27 all-atom force field was utilized for parameterization of the cyclic pentapeptide and all solvent molecules. The DG structures were first energy minimized *in vacuo*, then placed in truncated octahedral boxes with a minimum distance of 2.1 nm between solute atoms and the box walls. After the boxes were filled with solvent molecules, the systems were equilibrated with respect to temperature and pressure in subsequent steps, which are independently performed at increasing temperatures from 50 to 300 K in 50 K steps. A triple-range cutoff for Coulomb interactions including a reaction-field was used (0.8 and 1.4 nm). van der Waals interactions were calculated with a short-range cutoff of 0.8 nm and a long-range cutoff of 1.4 nm. An atom pair-list was used with a cutoff of 0.8 nm and was updated each five integration steps. All bonds were constrained with the SHAKE algorithm.[39] The integration time step was 2 fs. Each of the equilibration steps from 50 to 250 K had a run time of 50k ps and 0.5 ns for those at 300 K. The MD runs had a length of 2 ns. The output trajectories were then analyzed for internuclear distances and compared with the experimental data.

Homology Model—Chain R of the crystal structure of the activated β_2-adrenergic receptor (PDB ID 3SN6) was used as the template for secondary structural alignment in constructing the multiple sequence alignment (MSA). Seven other GPCR crystal structure sequences were included in the MSA (β_1-adrenergic receptors 2VT4 and 2Y00, A_2A receptors 2YDV, 3EML, and 3PWH, and β_2-adrenergic receptors 3KJ6 and 3P0G). In addition to the sequence from *Homo sapiens* (RefSeq ID NP_063941), MC3R sequences (AFH58736, AAI62747, AFH58735, NP_032587, ACK98821, AFH58734, NP_001020441, AAS66720, AFK25142, and ACK98822) from 10 other organisms were used. ClustalX[40] was used to generate the initial MSA, and manual alignment to the most highly conserved residue in each transmembrane helix (1.50, Asn93; 2.50, Asp121; 3.50, Arg179; 4.50, Trp206; 5.50, Met236; 6.50, Pro294; 7.50, Pro333, hMC3R numbering) was carried out in SeaView.[41] 3SN6 was also chosen as the template structure for homology model construction. MODELLER[42] was used to generate a set of 10 hMC3R models. The model that retained α-helical structure for all transmembrane helices, as well as the characteristic outward helical tilt and rotation in TM5 and TM6 of activated GPCRs, was selected for further loop refinement. All extracellular loops were simultaneously optimized using MODELLER, and the model chosen for docking studies had all extracellular loops pulled

away from the active site. This was chosen because previous studies had shown that extracellular loops had no effect on ligand binding to hMC3R.[43] Cytoplasmic loops were not optimized due to the fact that they are distal from the binding pocket, the focus of our study.

Ligand Construction—The 2-D MTII structure was obtained in .sdf format from PubChem and converted to three-dimensions and minimized in Avogadro.[44] SHU9119, peptide **15**, and peptide **17** structures were obtained based on NMR data obtained above and from previous work.[37,45]

Docking Protocol—Receptors and ligands were prepared for docking runs using the AutoDockTools4 (ADT) graphical user interface.[46] ADT was used to add hydrogen atoms, assign partial charges and atom types, and merge nonpolar hydrogen atoms into their respective heavy-atom bonded partners for the hMC3R homology model. Default settings were used to define rotatable bonds in each of the ligands to allow flexibility. The AutoDock/Vina plugin for PyMOL[47] was used to set parameters for the docking search space, which was a cube 33.75 Å in each direction, centered on the hMC3R binding pocket. AutodDock Vina[48] was used to perform molecular docking of ligands into the hMC3R binding pocket. Default settings were used, unless otherwise specified. Each Vina run produced nine clusters, and each ligand was run twice, for a total of 18 clusters per ligand. Results were visualized in PyMOL using the AutoDock/Vina plugin and analyzed for protein–ligand contacts with python scripts. AutoDock4[46] was used to calculate the binding energy and inhibition constants of each cluster from Vina.

RESULTS AND DISCUSSION

NMR Conformational Studies

NMR studies for the two peptides **15** and **17** in solution have been calculated by using the distance geometry (DG)[49] program with NOE-derived distances and $^{3}J_{H}$-coupling constant supported dihedral angles as structural restraints. In addition, the obtained structures were further analyzed by free or restrained (using the above derived NMR restraints) simulated annealing molecular dynamics (MD) calculations in GROMACS,[50–52] using the DG-derived NMR structure as the starting conformation. The analysis resulted in a preferred backbone conformation (Figure 2) for each of the peptides, exempting the side chain cyclized region consisting of the Lys^{10}-Asp^{4} residues.

The final structures for both the peptides presented a trans configuration for all the peptide bonds (Figure 2). The majority of NHs in both peptides have temperature coefficients ($\Delta\delta/\Delta T$) calculated for the backbone NHs over a temperature range of 295 to 315 K (Supporting Table 6) < –3.0 ppb/K in both the peptides, indicating solvent accessibility and that the NHs are not involved in strong intramolecular hydrogen bonding. For a comparative analysis of the conformations of **15**, **17**, and the parent peptides MTII and SHU9119, the (Φ,Ψ) dihedral space of all these peptides are represented as Ramachandran plots[53] (Figure 3 and Table 1). With the exception of Φ-Nle^{4},Ψ-Nle^{4}, and Φ-Asp^{5} which are external to the cyclic core of the peptides, the (Φ,Ψ) dihedral space for the cyclic region has mostly occupied the (−,+ quadrant) of the Ramachandran plot, corresponding to the β-sheet population. The

(**Φ**,**Ψ**) angles for nal[7] residues fall in the (+,− quadrant) diagonally opposite to the (−,+ quadrant), which is meaningful considering its opposite stereo configuration. Although the (**Φ**,**Ψ**) distribution for basic MTII and SHU9119 peptides is more centered in the β-sheet region, a downward shift of the overall distribution toward the overlapping β-sheet and α-helical regions is observed for **15** and **17**. None of the sequential (**Φ**,**Ψ**) patterns matched perfectly with any of the standard β-turn types.[53] However, the dihedral angles (**Φ**,**Ψ**) = (−78.7, 51.9) for His[6] in peptide **17** are characteristic of an inverted γ-turn centered around it, which facilitates nal[7]-NH-Asp[5]-CO hydrogen bonding. In support of this, a temperature coefficient of −3.0 ppb/K for nal[7]-NH signifies a relatively lower solvent accessibility compared to all other NHs and a probable participation in moderate hydrogen bonding. In contrast, this specific γ-turn structure is disrupted in **15** as evidenced from the (**Φ**,**Ψ**) = (−119.5, 36.4) about His[6]. This might be due to the N-methylation of the His[6]-NH which introduces a steric restriction to the peptide backbone and prevents an orientation of the Asp[5]-His[6] peptide bond that would normally be appropriate for nal[7]-NH-Asp[5]-CO hydrogen bonding. The temperature coefficient (−4.2 ppb/K) is in agreement for nal[7]-NH in **15**, proving its higher solvent accessibility in comparison to the corresponding nal[7]-NH in **17**.

The amino acid stretch His[6]-nal[7]-Arg[8]-Trp[9] forms a β-turn like structure (rather than a loop which usually requires more amino acids) in both the peptides with a turn on nal[7]-Arg[8]. The turn residues are flanked by His[6] and Trp[9] amino acids and are facing opposite to each other. The centering of the turn at nal[7]-Arg[8] can be explained by the conformational preference in general of consecutively located D-configured nal[7] and N-methylated Arg[8] amino acids. The corresponding dihedral space for the turn region in both peptides (Table 1) has a sign consistent with that of a type II' β turn observed for D-Pro-L-Pro [($\mathbf{\Phi}_{i+1}$,$\mathbf{\Psi}_{i+1}$,$\mathbf{\Phi}_{i+2}$,$\mathbf{\Psi}_{i+2}$) = (60°, − 120°, − 80°, 0)] but deviates in magnitude.[38,40] The distance between C_α atoms of His[6] and Trp[9] (6.12 and 7.17 Å, respectively, in **15** and **17**) is in agreement with the general definition of turns, providing further support for the validity of these structures.[55,56] In both peptides, the backbone region opposite nal[7]-Arg[8] comprised the side chains of Asp[5]-Lys[10] which are linked via side chain cyclization. Despite the linkage occurring between side chains, the distance between C_α atoms of Asp[5] and Lys[10] is 6.14 and 7.56 Å in **15** and **17**, similar to the distance between C_α atoms of His[6] and Trp[9]. This suggests the propagation of nal[7]-Arg[8] into an antiparallel β-sheet structure along the His[6] to Asp[5] and Trp[9] to Lys[10] on either side. However, the shorter residue–residue distance (~6 Å) in **15** compared to that in **17** (~7 Å) implies the constrained nature of the former structure. This increase in C_α separation in **17** also implies lengthened increase in overall size of the peptide. Most likely, this increase in size stems from the steric restrictions imposed by the three consecutive *N*-methyl groups on Arg[8], Trp[9], and Lys[10] of **17**. The orientation of *N*Me in Arg[8] is fixed by the conformational preorganization of the turn forming nal[7]-Arg[8] moiety, whereas the arrangement of *N*Me of Trp[9] into the cyclic core is necessitated both by the turn and the steric requirements from the *N*Me of Lys[10]. The absence of *N*Me on Trp[9] for **15** therefore results in a narrower structure. It is interesting to note the interplay of aromatic and van der Waals interactions in the nal[7]-Arg[8]-Trp[9] segment of **17**. A long-range π–π stacking interaction between the naphthyl group of nal[7] and the indole ring of Trp[9] is directly evidenced by the strikingly very low chemical shift (1.99 ppm) for the *N*Me on Arg[8], which is directly sandwiched between the two aromatic groups. The observed chemical shift is so

distinct that it is at least 0.7 ppm upfield of all other *N*Me in both peptides. In contrast, a normal chemical shift value of 2.87 ppm for *N*Me of Arg[8] in **15** implies the absence of such aromatic interactions as well as differences of orientation of the corresponding side chains. The overall twist in the backbone conformation of the two peptides leading to a completely different arrangement of functional side chains can be noted from the secondary structure representation in Figure 2c. Finally, comparison of backbone conformations for peptides **15** and **17** with the parent peptides MTII and SHU9119 reveal striking differences between the **Ψ** angles of nal[7] and Trp[9] (Table 1).

Molecular Dynamics Studies

The structures were further validated with MD simulations. Though the MD calculations without any restraints have been sufficient to further validate the DG structure for **17**, **15** required the usage of distance restraints within the cyclic region, which we speculate to be necessitated by the more constrained bent structure of **15**. Analysis of the MD trajectories for interproton distances (in angstoms, Supporting Tables 8 and 9) show good agreement with those calculated based on NOE data except for the distances between protons in the *N*-methyl groups, the indole NH of Trp[8], or the Nle[4]-NH. For all unviolated cases, the mean value for each interproton distance within ±10% of the corresponding distance was calculated from NMR and used in DG. The observed violations in specific cases are attributed to the presence of Nle[4]-NH in a conformationally flexible region and the exchanging nature of the indole NH of Trp[9]. The stability of the backbone conformations for both peptides is further illustrated by the conserved dihedral angle distribution in the respective MD studies (Supporting Figures 2–5), which are within ±30° of the dihedral angles measured from the corresponding DG structures. However, as expected, variation in the distribution is observed for the side chain cyclized region.

The χ_1 rotamer populations for the side chain conformations of all the amino acids were analyzed from the MD simulations. They were also experimentally determined based on the homonuclear $^3J_{H\alpha\text{-}H\beta}$ and heteronuclear couplings $^3J_{C'\text{–}H\beta 1,2}$ and NOE data of the stereospecifically assigned β-protons wherever possible (see Supporting Information).[41,42] The absence of low $^3J_{H\alpha\text{-}H\beta}$ coupling constants and their sum >13 Hz in each of the amino acids suggests a complete predominance of the $\chi_1 = +60°$ conformation for L-amino acids and the $\chi_1 = -60°$ conformation for D-amino acids. The discrete $^3J_{H\alpha\text{-}H\beta}$ values (but without an extreme difference of 9 Hz) observed for each residue is therefore a result of a mix of populations: mostly $\chi_1 = -60°$ ($\chi_1 = +60°$ for D-amino acids) along with $\chi_1 = 180°$. This result is also corroborated by our MD simulations. For Asp[5], the NMR data imply $\chi_1 = 180°$ and $\chi_1 = -60°$ as the most predominant conformations in **15** ($J_{H\alpha\text{-}H\beta pro\text{-}R} = 4.9$ Hz and $J_{H\alpha\text{-}H\beta pro\text{-}S} = 10.2$ Hz) and **17** ($J_{H\alpha\text{-}H\beta pro\text{-}R} = 9.1$ Hz and $J_{H\alpha\text{-}H\beta pro\text{-}S} = 5.1$ Hz), respectively, and this result is also reproduced by the MD simulations. This distinct χ_1 distribution for Asp[5] in **15** and **17** may stem from the conformational requirements of the cyclical peptidic core, as Asp[5] forms an integral part of the cyclic core via side chain cyclization with the Lys[10] side chain. NMR data for nal[7] (with larger $J_{H\alpha\text{-}H\beta pro\text{-}S} = 9.0$ and 8.7 Hz coupling constants in **15** and **17**, respectively) predicts $\chi_1 = 60°$ as the major conformation in both peptides. Although the MD simulations show a similar population distribution in **15**, a higher population of $\chi_1 = 180°$ exists for **17**. Lys[10] in **15** exhibits a dynamical nature with

almost equally populated χ_1 rotamers in contrast to that in **17**, with a strong preference for $\chi_1 = -60°$. These varying conformations for peptides **15** and **17** demonstrate the conformational modulation in the SHU9119 backbone generated by N-methylation and are the key to differential interactions with melanocortin receptor subtypes and corresponding activity responses.

Docking Studies of Peptide 15 and Peptide 17

To understand the implications of the structural dissimilarities of **15** and **17** on their interactions with hMC3R, we performed docking simulations of MTII, SHU9119, and peptides **15** and **17** into our homology model of hMC3R. The docking studies showed a good overall agreement with hMC3R mutation studies, a previous study from Chen et al. which identified several residues in hMC3R that directly affect agonist/ antagonist binding and receptor activity.[38] Of the residues identified, all but two (D121 and D332) are proximal to the hMC3R binding pocket in our homology model. All clusters (total 18) for each ligand were analyzed to detect contacts within 4.0 Å of the mutated amino acids (Figure 4). Each ligand interacts with D154 and D158, consistent with the study by Chen et al., which showed that the mutation of D154 or D158 leads to dramatically decreased binding affinity and receptor signaling.[38] Our docking results also show that D154/D158 has the highest contacts with all four peptides (MTII, SHU9119, peptide **15**, and peptide **17**) and indicate that D154/D158 is critical for ligand binding to hMC3R. In the majority of cases, H298 was not in close contact with ligands, which is in contrast to the results of Chen et al. However, slight differences have also been seen between binding of MTII and the SHU9119 N-methylated compounds: F295 was in contact with MTII in over 80% of the clusters, whereas less than 60% of SHU9119 and peptide **17** clusters and about 20% of peptide **15** clusters are in close proximity to F295, indicating that F295 is important for hMC3R agonist activity. These results agree with the binding affinities of MTII, SHU9119, peptide **17**, and peptide **15** with 2 nM, 3.7 nM, 9.7 nM, and 15 nM, respectively, to hMC3R. In addition, E131 did not play a significant role in MTII binding (about 35% contact rate) but is observed to be in contact with more than half the clusters of the SHU ligands indicating that E131 is important for the antagonist activities of SHU9119 and peptides **15** and **17**.

Another important aspect from the Chen et al. study is the identification of amino acid residues in the cyclic peptide ligands that were most responsible for binding and activity, showing that the -D-Phe^7-Arg^8-Trp^9- tripeptide was the smallest fragment that could still bind and activate hMC3R.[38] Each ligand tested confirms this result; D-Phe^7 (or nal in the case of SHU9119 and peptides **15** and **17**), Arg^8, and Trp^9 are the residues with the highest average number of contacts (total number of interactions within 4.0 Å between ligand atoms and any atom in hMC3R, averaged over 18 clusters) (Figure 5). Slight differences exist among the ligands, as Arg^8 has the most ligand–receptor contacts for MTII, peptide **17**, and peptide **15**, whereas nal^7 has the highest number of contacts for SHU9119. In addition, Trp^9 has very high contacts (>40) with hMC3R for SHU9119, peptide **15** and **17** but not for MT-II, indicating that Trp^9 plays an important role in antagonist activity of hMC3R.

From our docking studies, it is clear that polar and aromatic interactions play an important role in ligand binding to hMC3R. Inspection of individual ligand–receptor complexes

reveals subtle differences for MTII, SHU9119, and peptides **15** and **17**. The best docked complex for the agonist MTII (nM binding affinity (K_i)) forms polar contacts with D154 and D158 through the side chains of Arg^8 (Figure 6a). In addition, polar contacts are formed between Q151 and Arg^8 and between D158 and the backbone of D-Phe^7. π–π stacking, which stabilizes interactions between aromatic amino acid side chains,[57] is also present in the MTII-hMC3R complex. D-Phe^7 inserts itself most deeply into the hMC3R binding pocket, forming T-shaped stacking with the aromatic side chains of F295, F296, and F318 on TM6 and TM7. In contrast, the antagonist, SHU9119 (nM K_i), is rotated within the hMC3R binding pocket. Polar interactions with D154 and D158 are still present but are with Asp^5 and Arg^8, respectively (Figure 6b). An additional polar contact exists between the carbonyl group of the I217 backbone and the terminal amino group of SHU9119. No penetration into the deepest part of the binding pocket is present with SHU9119, but a T-shaped stacking interaction is formed between nal^7-F318-Trp^9. Another possible T-shaped interaction could be formed between nal^7 and either Y310 or Y314, which are located in the extracellular loop 3 (EL3), but verification has been limited by the AutoDockVina models which require a rigid protein backbone for hMC3R.

Peptides **17** and **15**, the methylated analogues of SHU9119, share some of the characteristic nonbonded interactions present for both MTII and SHU9119 binding to hMC3R. Peptide **17** forms an extensive network of polar contacts with Q151, D154, and D158 through its Arg^8 side chain (Figure 6c). Additionally, there are also polar contacts existing on that side of the hMC3R binding pocket between the backbone of Asp^5 and the side chains of D154 and D158, as well as between the N-terminal carbonyl and the side chain of E131. Similar to MTII, peptide **17** also wedges the nal^7 residue into the deepest part of the binding pocket, forming T-shaped stacking interactions with F295 and F296. However, Trp^9 has stacking interactions with F318, similar to SHU9119. Again, Y310 and Y314 could potentially form stacking interactions with Trp^9, but they lie just outside the 5 Å range typical of π–π stacking.

The weakest binder is peptide **15**, most likely due to its orientation inside the binding pocket, different from that of MTII, SHU9119, and peptide **17**. Polar contacts were again formed with Arg^8 but between the carbonyl backbone and side chains of Q151 and D154 (Figure 6d). Side chain polar contacts were only formed between Arg^8 and D158. S220 also forms a polar contact with the acetyl group of the N-terminus. F318 is close enough to create stacking interactions but is not orthogonal or parallel to nal^7, a prerequisite for π–π stacking. Finally, Y219 could potentially form stacking interactions with Trp^9 but is rotated away from the binding pocket.

CONCLUSIONS

Exploitation of the melanocortin system for drug development to combat various diseases has been a great challenge due to the lack of extensive information about the structural requirements of ligands that lead to selectivity of hMCRs. This in turn is a result of the lack of hMCR subtype-selective ligands. In our studies on N-methylated libraries of the SHU9119 cyclic peptide, we have developed two conformationally constrained analogues (namely, **15** and **17**) that are selective for the hMC3R subtype, enabling us to investigate the

structural aspects of ligand–hMC3R interaction. The conformation of peptides **15** and **17** demonstrated that Trp^9 is significantly different from the cyclic peptide agonist MTII. Molecular docking studies of MTII, SHU9119, peptide **15**, and peptide **17** reveal that Arg^8 is critical for binding with D154 and D158 of hMC3R. The docking studies further indicate that as Trp^9 increases interactions with F295 in hMC3R, agonist activity can also be expected to increase. These results strengthen our earlier discovery of D-Trp^8- -MSH as a selective agonist of hMC3R. Furthermore, E131 in hMC3R is seen to be important for antagonist activities of SHU9119 as well as of peptides **15** and **17**. This study provides compelling evidence that molecular–receptor interactions studies using a combination of a chimeric receptor, NMR spectroscopy, and docking strategies will enhance the rational design of selective antagonists of hMC3R.

Supplementary Material

Refer to Web version on PubMed Central for supplementary material.

Acknowledgments

Funding

This study was supported in part by grants from the U.S. Public Health Service, National Institutes of Health, DK017420, GM 108040, and DA06284. We thank IGSSE (International Graduate School of Science and Engineering), the Bund der Freunde der TU Münchene.V., CompInt (Materials Science of Complex Interfaces) of the Elite Network of Bavaria for funding and IAS (Institute for Advanced Study) of Technische Universität München, CIPSM (Center for Integrated Protein Science Munich), and Deutsche Forschungsgemeinschaft for a Koselleck grant.

ABBREVIATIONS

hMCR	human melanocortin receptor
MTII	Melanotan II
TM	transmembrane

References

1. Getting SJ. Targeting melanocortin receptors as potential novel therapeutics. Pharmacol Ther. 2006; 111:1–15. [PubMed: 16488018]
2. Cai M, Nyberg J, Hruby VJ. Melanotropins as drugs for the treatment of obesity and other feeding disorders: potential and problems. Curr Top Med Chem. 2009; 9:554–563. [PubMed: 19689365]
3. Hadley ME, Hruby VJ. The Melanotropic Peptides. Am Zool. 1986; 26:A28–A28.
4. Hadley ME, Sharma SD, Hruby VJ, Levine N, Dorr RT. Melanotropic Peptides for Therapeutic and Cosmetic Tanning of the Skin. Ann N Y Acad Sci. 1993; 680:424–439. [PubMed: 8390162]
5. Abdel-Malek Z, Suzuki I, Tada A, Im S, Akcali C. The melanocortin-1 receptor and human pigmentation. Ann N Y Acad Sci. 1999; 885:117–133. [PubMed: 10816645]
6. Jiang JW, Sharma SD, Nakamura S, Lai JY, Fink JL, Hruby VJ, Hadley ME. The melanotropic peptide, [Nle(4),D-Phe(7)]alpha-MSH, stimulates human melanoma tyrosinase activity and inhibits cell proliferation. Pigm Cell Res. 1995; 8:314–323.
7. Brzoska T, Bohm M, Lugering A, Loser K, Luger TA. Terminal signal: anti-inflammatory effects of alpha-melanocyte-stimulating hormone related peptides beyond the pharmacophore. Adv Exp Med Biol. 2010; 681:107–116. [PubMed: 21222263]

8. Muceniece R, Dambrova M. Melanocortins in brain inflammation: the role of melanocortin receptor subtypes. Adv Exp Med Biol. 2010; 681:61–70. [PubMed: 21222260]
9. Wessells H, Fuciarelli K, Hansen J, Hadley ME, Hruby VJ, Dorr R, Levine N. Synthetic melanotropic peptide initiates erections in men with psychogenic erectile dysfunction: double-blind, placebo controlled crossover study. J Urol. 1998; 160:389–393. [PubMed: 9679884]
10. Ni XP, Butler AA, Cone RD, Humphreys MH. Central receptors mediating the cardiovascular actions of melanocyte stimulating hormones. J Hypertens. 2006; 24:2239–2246. [PubMed: 17053546]
11. Li SJ, Varga K, Archer P, Hruby VJ, Sharma SD, Kesterson RA, Cone RD, Kunos G. Melanocortin antagonists define two distinct pathways of cardiovascular control by alpha- and gamma-melanocyte-stimulating hormones. J Neurosci. 1996; 16:5182–5188. [PubMed: 8756446]
12. Fan W, Boston BA, Kesterson RA, Hruby VJ, Cone RD. Role of melanocortinergic neurons in feeding and the agouti obesity syndrome. Nature. 1997; 385:165–168. [PubMed: 8990120]
13. Cone RD. The central melanocortin system and its role in energy homeostasis. Ann Endocrinol (Paris). 1999; 60:3–9. [PubMed: 10374010]
14. Butler AA, Cone RD. Knockout studies defining different roles for melanocortin receptors in energy homeostasis. Ann N Y Acad Sci. 2003; 994:240–245. [PubMed: 12851322]
15. Krashes MJ, Lowell BB, Garfield AS. Melanocortin-4 receptor-regulated energy homeostasis. Nat Neurosci. 2016; 19:206–219. [PubMed: 26814590]
16. Murphy B, Nunes CN, Ronan JJ, Harper CM, Beall MJ, Hanaway M, Fairhurst AM, Van der Ploeg LHT, MacIntyre DE, Mellin TN. Melanocortin mediated inhibition of feeding behavior in rats. Neuropeptides. 1998; 32:491–497. [PubMed: 9920446]
17. Morgan C, Thomas RE, Cone RD. Melanocortin-5 receptor deficiency promotes defensive behavior in male mice. Horm Behav. 2004; 45:58–63. [PubMed: 14733892]
18. Morgan C, Thomas RE, Ma WD, Novotny MV, Cone RD. Melanocortin-5 receptor deficiency reduces a pheromonal signal for aggression in male mice. Chem Senses. 2004; 29:111–115. [PubMed: 14977807]
19. van der Kraan M, Tatro JB, Entwistle ML, Brakkee JH, Burbach JPH, Adan RAH, Gispen WH. Expression of melanocortin receptors and pro-opiomelanocortin in the rat spinal cord in relation to neurotrophic effects of melanocortins. Mol Brain Res. 1999; 63:276–286. [PubMed: 9878783]
20. Juni A, Cai MY, Stankova M, Waxman AR, Arout C, Klein G, Dahan A, Hruby VJ, Mogil JS, Kest B. Sex-specific Mediation of Opioid-induced Hyperalgesia by the Melanocortin-1 Receptor. Anesthesiology. 2010; 112:181–188. [PubMed: 19996949]
21. Vrinten DH, Kalkman CJ, Adan RAH, Gispen WH. Neuropathic pain: a possible role for the melanocortin system? Eur J Pharmacol. 2001; 429:61–69. [PubMed: 11698027]
22. Mogil JS, Ritchie J, Smith SB, Strasburg K, Kaplan L, Wallace MR, Romberg RR, Bijl H, Sarton EY, Fillingim RB, Dahan A. Melanocortin-1 receptor gene variants affect pain and mu-opioid analgesia in mice and humans. J Med Genet. 2005; 42:583–587. [PubMed: 15994880]
23. Chu HC, Xia JL, Xu HM, Yang Z, Gao J, Liu SH. Melanocortin 4 Receptor Mediates Neuropathic Pain Through p38MAPK in Spinal Cord. Can J Neurol Sci. 2012; 39:458–464. [PubMed: 22728852]
24. Srinivasan S, Vaisse C, Conklin BR. Engineering the melanocortin-4 receptor to control G(s) signaling in vivo. Ann N Y Acad Sci. 2003; 994:225–232. [PubMed: 12851320]
25. Hadley ME, Haskell-Luevano C. The proopiomelanocortin system. Ann N Y Acad Sci. 1999; 885:1–21. [PubMed: 10816638]
26. Fekete C, Sarkar S, Rand WM, Harney JW, Emerson CH, Bianco AC, Lechan RM. Agouti-related protein (AGRP) has a central inhibitory action on the hypothalamic-pituitary-thyroid (HPT) axis; Comparisons between the effect of AGRP and neuropeptide Y on energy homeostasis and the HPT axis. Endocrinology. 2002; 143:3846–3853. [PubMed: 12239096]
27. Fekete C, Marks DL, Sarkar S, Emerson CH, Rand WM, Cone RD, Lechan RM. Effect of Agouti-related protein in regulation of the hypothalamic-pituitary-thyroid axis in the melanocortin 4 receptor knockout mouse. Endocrinology. 2004; 145:4816–4821. [PubMed: 15256492]

28. Tota MR, Smith TS, Mao C, MacNeil T, Mosley RT, Van der Ploeg LHT, Fong TM. Molecular interaction of Agouti protein and Agouti-related protein with human melanocortin receptors. Biochemistry. 1999; 38:897–904. [PubMed: 9893984]
29. Chen M, Cai M, Aprahamian CJ, Georgeson KE, Hruby V, Harmon CM, Yang Y. Contribution of the conserved amino acids of the melanocortin-4 receptor in [Nle4, D-Phe(7)]-alpha-melanocytestimulating hormone binding and signaling. J Biol Chem. 2007; 282:21712–21719. [PubMed: 17545153]
30. Yang Y, Fong TM, Dickinson CJ, Mao C, Li JY, Tota MR, Mosley R, Van der Ploeg LHT, Gantz I. Molecular determinants of ligand binding to the human melanocortin-4 receptor. Biochemistry. 2000; 39:14900–14911. [PubMed: 11101306]
31. Chen M, Cai MY, McPherson D, Hruby V, Harmon CM, Yang YK. Contribution of the transmembrane domain 6 of melanocortin-4 receptor to peptide [Pro(5), DNa1 (2 ') (8)]-gamma-MSH selectivity. Biochem Pharmacol. 2009; 77:114–124. [PubMed: 18930713]
32. Yang YK, Cai MY, Chen M, Qu HC, McPherson D, Hruby V, Harmon CM. Key amino acid residues in the melanocortin-4 receptor for nonpeptide THIQ specific binding and signaling. Regul Pept. 2009; 155:46–54. [PubMed: 19303903]
33. Montero-Melendez T, Gobbetti T, Cooray SN, Jonassen TEN, Perretti M. Biased Agonism as a Novel Strategy To Harness the Proresolving Properties of Melanocortin Receptors without Eliciting Melanogenic Effects. J Immunol. 2015; 194:3381–3388. [PubMed: 25725103]
34. Yang YK, Chen M, Dimmitt R, Harmon CM. Structural Insight into the MC4R Conformational Changes via Different Agonist-Mediated Receptor Signaling. Biochemistry. 2014; 53:7086–7092. [PubMed: 25347793]
35. Huang H, Tao YX. A Small Molecule Agonist THIQ as a Novel Pharmacoperone for Intracellularly Retained Melanocortin-4 Receptor Mutants. Int J Biol Sci. 2014; 10:817–824. [PubMed: 25076858]
36. Molden BM, Cooney KA, West K, Van Der Ploeg LHT, Baldini G. Temporal cAMP Signaling Selectivity by Natural and Synthetic MC4R Agonists. Mol Endocrinol. 2015; 29:1619–1633. [PubMed: 26418335]
37. Cai M, Marelli UK, Bao J, Beck JG, Opperer F, Rechenmacher F, McLeod KR, Zingsheim MR, Doedens L, Kessler H, Hruby VJ. Systematic Backbone Conformational Constraints on a Cyclic Melanotropin Ligand Leads to Highly Selective Ligands for Multiple Melanocortin Receptors. J Med Chem. 2015; 58:6359–6367. [PubMed: 26218460]
38. Chen M, Aprahamian CJ, Celik A, Georgeson KE, Garvey WT, Harmon CM, Yang YK. Molecular characterization of human melanocortin-3 receptor ligand-receptor interaction. Biochemistry. 2006; 45:1128–1137. [PubMed: 16430209]
39. Ryckaert JP, Ciccotti G, Berendsen HJC. Numerical-Integration of Cartesian Equations of Motion of a System with Constraints - Molecular-Dynamics of N-Alkanes. J Comput Phys. 1977; 23:327–341.
40. Larkin MA, Blackshields G, Brown NP, Chenna R, McGettigan PA, McWilliam H, Valentin F, Wallace IM, Wilm A, Lopez R, Thompson JD, Gibson TJ, Higgins DG. Clustal W and clustal X version 2.0. Bioinformatics. 2007; 23:2947–2948. [PubMed: 17846036]
41. Gouy M, Guindon S, Gascuel O. SeaView Version 4: A Multiplatform Graphical User Interface for Sequence Alignment and Phylogenetic Tree Building. Mol Biol Evol. 2010; 27:221–224. [PubMed: 19854763]
42. Baxevanis AD. The importance of biological databases in biological discovery. Curr Protoc Bioinformatics. 2006; Chapter 1doi: 10.1002/0471250953.bi0101s13
43. Bolton EE, Wang YL, Thiessen PA, Bryant SH. PubChem: Integrated Platform of Small Molecules and Biological Activities. Annu Rep Comput Chem. 2008; 4:217–241.
44. Hanwell MD, Curtis DE, Lonie DC, Vandermeersch T, Zurek E, Hutchison GR. Avogadro: an advanced semantic chemical editor, visualization, and analysis platform. J Cheminf. 2012; 4:17.
45. Ying JF, Kover KE, Gu XY, Han GX, Trivedi DB, Kavarana MJ, Hruby VJ. Solution structures of cyclic melanocortin agonists and antagonists by NMR. Biopolymers. 2003; 71:696–716. [PubMed: 14991679]

46. Morris GM, Huey R, Lindstrom W, Sanner MF, Belew RK, Goodsell DS, Olson AJ. AutoDock4 and AutoDockTools4: Automated Docking with Selective Receptor Flexibility. J Comput Chem. 2009; 30:2785–2791. [PubMed: 19399780]

47. Seeliger D, de Groot BL. Ligand docking and binding site analysis with PyMOL and Autodock/Vina. J Comput-Aided Mol Des. 2010; 24:417–422. [PubMed: 20401516]

48. Trott O, Olson AJ. AutoDock Vina: Improving the Speed and Accuracy of Docking with a New Scoring Function, Efficient Optimization, and Multithreading. J Comput Chem. 2010; 31:455–461. [PubMed: 19499576]

49. Havel TF. An Evaluation of Computational Strategies for Use in the Determination of Protein-Structure from Distance Constraints Obtained by Nuclear-Magnetic-Resonance. Prog Biophys Mol Biol. 1991; 56:43–78. [PubMed: 1947127]

50. Lindahl E, Hess B, van der Spoel D. GROMACS 3.0: a package for molecular simulation and trajectory analysis. J Mol Model. 2001; 7:306–317.

51. Van der Spoel D, Lindahl E, Hess B, Groenhof G, Mark AE, Berendsen HJC. GROMACS: Fast, flexible, and free. J Comput Chem. 2005; 26:1701–1718. [PubMed: 16211538]

52. Beck, JF., Frank, AO., Kessler, H. NMR of Biomolecules: Towards Mechanistic Systems Biology. Wiley; New York: 2012. NMR of Peptides.

53. Chou KC. Prediction of tight turns and their types in proteins. Anal Biochem. 2000; 286:1–16. [PubMed: 11038267]

54. Doedens L, Opperer F, Cai MY, Beck JG, Dedek M, Palmer E, Hruby VJ, Kessler H. Multiple N-Methylation of MT-II Backbone Amide Bonds Leads to Melanocortin Receptor Subtype hMC1R Selectivity: Pharmacological and Conformational Studies. J Am Chem Soc. 2010; 132:8115–8128. [PubMed: 20496895]

55. Nair CM, Vijayan M, Venkatachalapathi YV, Balaram P. X-Ray Crystal-Structure of Pivaloyl-D-Pro-L-Pro-L-Ala-N-Methylamide - Observation of a Consecutive Beta-Turn Conformation. J Chem Soc, Chem Commun. 1979:1183–1184.

56. Gibbs AC, Bjorndahl TC, Hodges RS, Wishart DS. Probing the structural determinants of type II ' beta-turn formation in peptides and proteins. J Am Chem Soc. 2002; 124:1203–1213. [PubMed: 11841288]

57. Chelli R, Gervasio FL, Procacci P, Schettino V. Stacking and T-shape competition in aromatic-aromatic amino acid interactions. J Am Chem Soc. 2002; 124:6133–6143. [PubMed: 12022848]

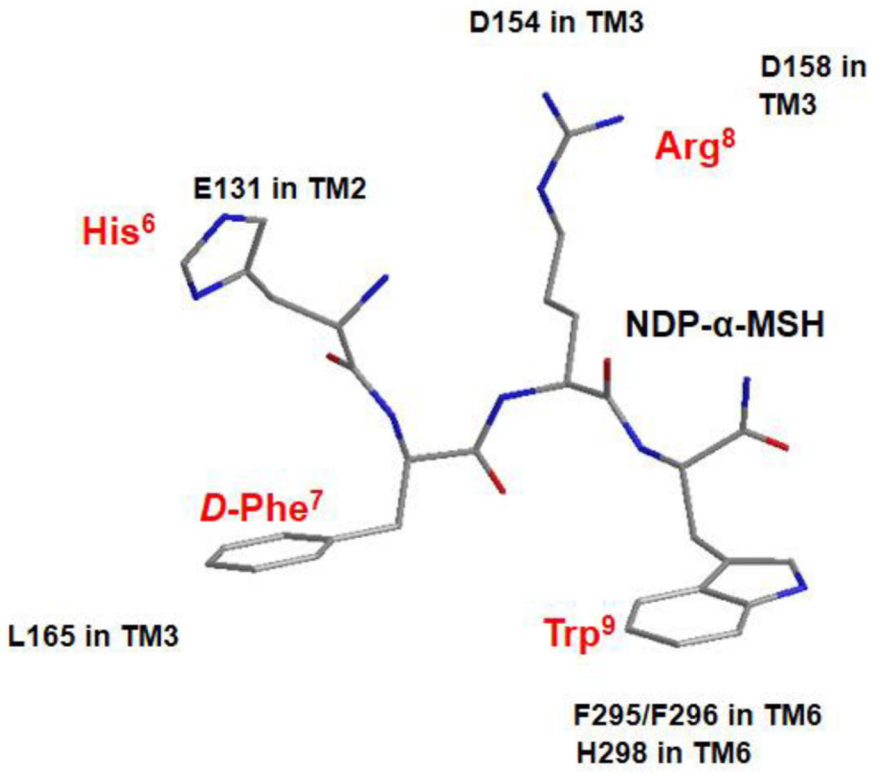

Figure 1.

Model for receptor–ligand complexation in hMC3R activation. Two-dimensional representation of a proposed three-dimensional model illustrating the synthetic melanocortin NDP-α-MSH bound to hMC3R. Two major receptor binding sites are hypothesized, with the first being a predominantly ionic pocket formed by D154 and D158, and the second a hydrophobic pocket formed by aromatic residues in TM6.[29–32]

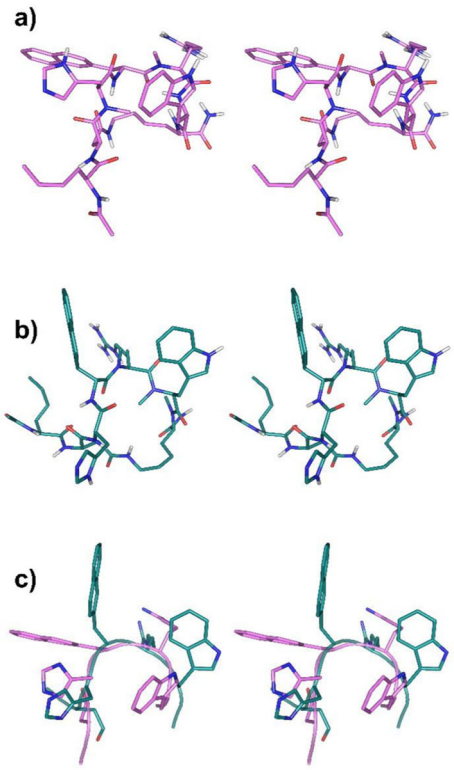

Figure 2.

NMR structures of hMC3R peptides **15** and **17**. Stereo views of the NMR structure of peptides **15** (a, pink); **17** (b, green); and the overlay of the β-turn like His^{6}-nal^{7}-Arg^{8}-Trp^{9} region from peptides **15** and **17** (c). Ribbons along backbones highlight secondary structural features. For clarity, nonpolar hydrogens in a and b are shown, whereas all the hydrogens and the main chain in c are not shown.

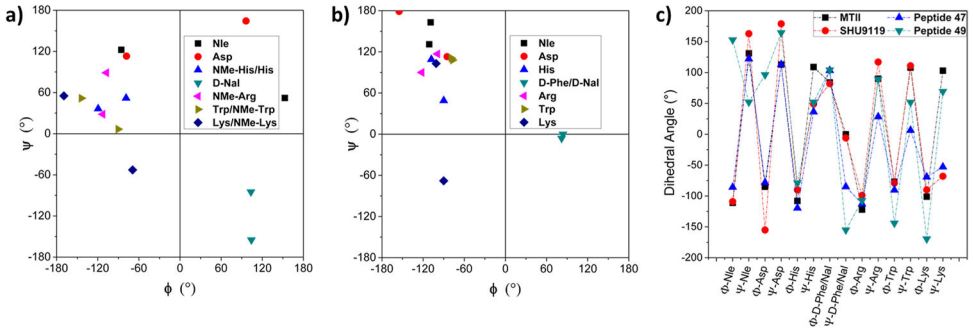

Figure 3.

Backbone conformations of peptides 15 and 17 are largely consistent with hMC3R ligands MTII and SHU9119, with a few notable differences. Ramachandran plots that represent the (**Φ**,**Ψ**) dihedral space of constituent amino acids and corresponding secondary structural information, generated for (a) peptides **15** and **17** based on their NMR structures and (b) for peptides **MTII** and **SHU9119**. (c) Graph showing the site-specific variations in the dihedral space.

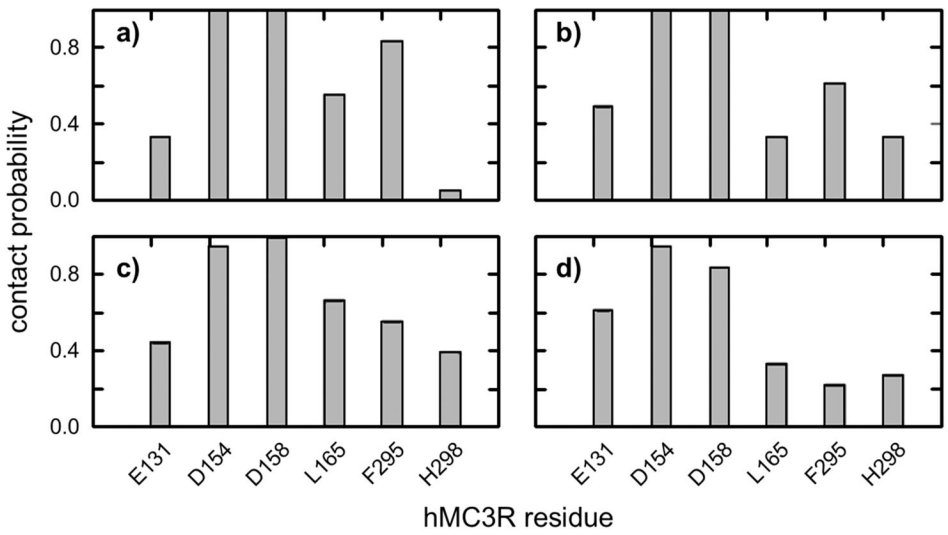

Figure 4.

Docked ligands interact with hMC3R residues that are crucial for ligand binding and activity. (a) Contact probability (calculated as percentage of docking clusters with ligand atoms within 4.0 Å of specified hMC3R residue) of MTII to interact with functionally important residues in hMC3R. (b) Contact probability of SHU9119 with residues in hMC3R. (c) Contact probability for peptide **15**. (d) Contact probability for peptide **17**.

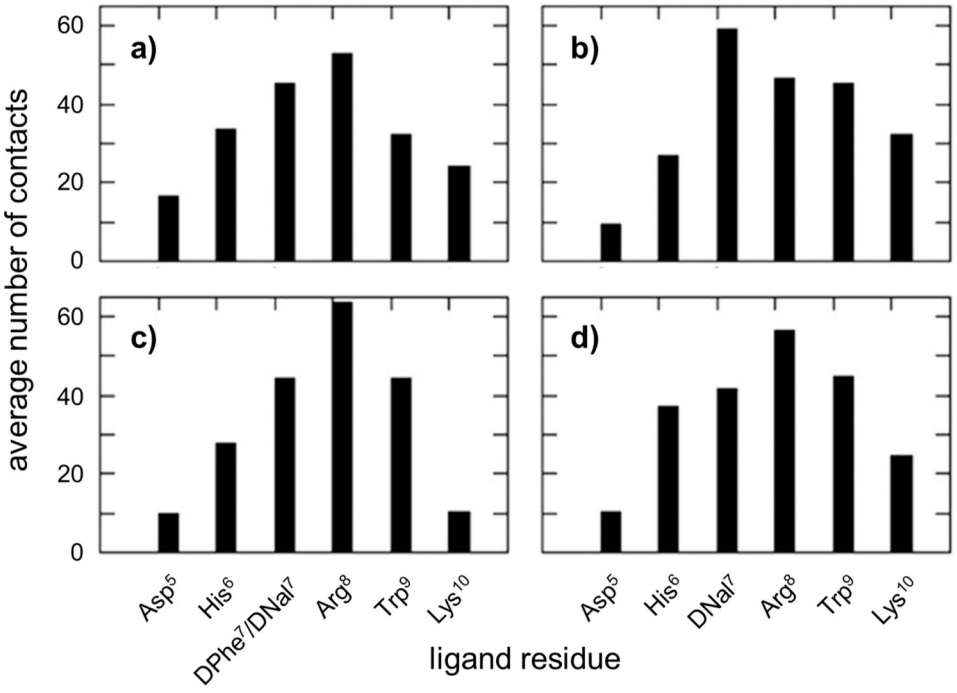

Figure 5.

N-methylation modulates localized effectiveness of binding in SHU9119 analogues. (a) Per-residue number of contacts between MTII and hMC3R in docking studies. Average number of contacts is defined as total number of interactions within 4.0 Å between ligand atoms and any atom in hMC3R averaged over 18 docking clusters. Residue seven is DPhe in MTII (a) and DNal in peptide **15** (c). (b) Per-residue number of contacts between SHU9119 and hMC3R. (c) Per-residue number of contacts between peptide **15** and hMC3R. (d) Per-residue number of contacts between peptide **17** and hMC3R.

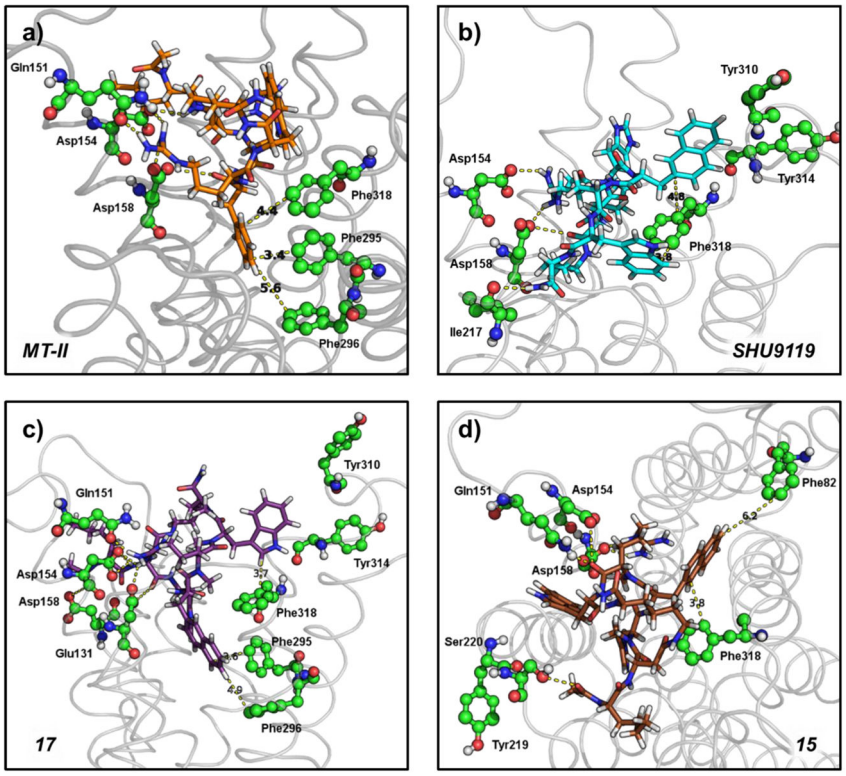

Figure 6.

Polar and π–π interactions stabilize binding of ligands to the hMC3R binding pocket. (a) Snapshot of lowest-energy binding complex between MTII and hMC3R. (b) Snapshot of lowest-energy binding complex between SHU9119 and hMC3R. (c) Snapshot of lowest-energy binding complex between peptide **17** and hMC3R. (d) Snapshot of the lowest-energy binding complex between peptide **15** and hMC3R. Sticks, docked ligands; ball and sticks, hMC3R amino acid residues; dashes, nonbonded interactions between ligand and receptor <5 Å; gray ribbons, cartoon representation of hMC3R; red, oxygen atoms; blue, nitrogen; white, hydrogen; green, carbons in hMC3R; orange, MTII carbons; cyan, SHU9119 carbons; purple, peptide **17** carbons; brown, peptide **15** carbons. All complexes were rendered in PyMOL.

Table 1

(Φ,Ψ) Dihedral Angles at Each of the Constituent Amino Acids As Measured from the NMR Structures of the Following Peptides

	Nle[4]		Asp[5]		His[6]		d-Phe[7]/nal[7]		Arg[8]		Trp[9]		Lys[10]	
compound	**Φ**	**Ψ**	**Φ**	**Ψ**	**Φ**	**Ψ**	**Φ**	**Ψ**	**Φ**	**Ψ**	**Φ**	**Ψ**	**Φ**	**Ψ**
peptide 15	−85.7	122.3	−78.1	113.1	−119.5	36.4	103.4	−84.9	−112.8	28.4	−90.3	6.5	−69.2	−52.8
peptide 17	152.9	52.1	96.3	164.4	−78.7	51.9	104.1	−155.0	−107.4	88.9	−144.0	51.7	−169.5	69.3
MTII[a]	−111.0	131.0	−85.0	113.0	−108	109.0	84.0	0.0	−122.0	90.0	−77.0	108.0	−101.0	103.0
SHU9119[a]	−109.0	163.0	−155.0	179.0	−90.0	49.0	82.0	−6.0	−99.0	117.0	−79.0	111.0	−90.0	−68.0
MTII(*N*Me)[b]	−101.0	109.1	71.4	143.7	−97.8	78.4	96.1	−125.9	−135.2	80.4	−119.8	62.6	−113.7	0.4

[a] Structural data published in earlier work.[45]

[b] MTII(*NMe*): N-methylated MTII, Ac-Nle-c[Asp-*NMe* His-DPhe-*NMe* Arg-*NMe* Trp-*NMe*Lys]-NH2. Data published in previous work,[54] corresponding to peptide **28**.